Progress In Electromagnetics Research, Vol. 132, 479–498, 2012

PERFORMANCE EVALUATION OF UWB ON-BODY COMMUNICATION UNDER WIMAX OFF-BODY EMI EXISTENCE

A.-M. Gao*, Q.-H. Xu, H.-L. Peng, W. Jiang, and Y. Jiang

Key Lab of Ministry of Education for Design and EMC of High-Speed Electronic Systems, Shanghai Jiao Tong University, Shanghai 200240, China

Abstract—A study of UWB on-body communication system performance, with the WiMax off-body electromagnetic interference (EMI) existence, is presented. Firstly, a compact UWB antenna with good on-body performance is verified and chosen as our reference antenna. Using this realistic antenna, channel transfer function (CTF) of UWB on-body channel in an indoor room is investigated by measurements. Based on the measured data, the parameters of its pathloss model and its power delay profile (PDP) model are extracted respectively. Secondly, a new body channel communication system model, composed of the on-body and off-body dual-link channel, together with UWB and WiMax signal models are presented. Finally, UWB on-body communication performances under different WiMax off-body EMI levels are studied by simulation. Simulated results show that this on-body system performance is quite limited and easily affected by the off-body WiMax EMI. It is pointed out that the existing UWB on-body communication abilities should be greatly improved when WiMax off-body EMI signals are considered.

1. INTRODUCTION

Wireless body area network (WBAN) refers to wireless network among wearable and/or implantable sensors located on, off, or in the body. WBAN has been found widely applications in biomedical therapy, healthcare and entertainment [1–3]. Therefore, during the last decade many researchers have paid great attention to developing its system technologies which have been conducted in several directions, such

Received 19 August 2012, Accepted 28 September 2012, Scheduled 9 October 2012

* Corresponding author: An-Ming Gao (annmean@163.com).

as on- or off-body wearable antenna design and optimization [4–9], WBAN body channel modeling [10, 11], and analysis of the effects of human body on wireless links performance [12, 13]. Moreover, it has been fully understood that the essential functionality of WBAN is transferring human body information data, which makes the data communication with features of low power, immediacy and convenience be highly expected for WBAN system.

It is known that UWB has been considered by IEEE as one of the promising candidates for WBAN applications because of its above features [14, 15]. Therefore, many researchers today have paid great attention to UWB-WBAN communications, of which designing UWB on-body antenna [16–23], modeling UWB body channel model [24–26], and evaluating on-body UWB communication system performance [27, 28] are the most concerned. These researches provided a strong and well-understood basis for the WBAN development. However, to the authors' knowledge, less work has been done when transmission performance of on-body UWB system under WiMax EMI existence are concerned. On-body UWB/off-body WiMax dual-model and dual-link (DM-DL) in which case the two modes are working at the same time and the received signal of WiMax is an EMI to UWB is the development trend in future UWB WBAN, investigation on this topic is of significance to the development of a realistic UWB WBAN system. This is the main motivation behind this paper.

The organization of this paper is arranged as follows. In Section 2, UWB/WiMax dual-link body channel model and dual-mode signal model are investigated. Some key issues for pathloss and power delay profile of UWB on-body channel are developed experimentally with their extracted parameters presented. The dual-mode signal models are also described in details by mathematical expressions. In Section 3, UWB WBAN BER characteristics in DM-DL scenario are studied by using system level simulations. Their results of the system performance for our on-body UWB communication system under WiMax EMI are obtained and analyzed. Conclusions are finally drawn in Section 4.

2. CHANNEL AND SIGNAL MODELING

2.1. Dual-link Body Channel

Our dual-link body channel model includes UWB on-body channel model and WiMax off-body channel model. Between them, the WiMax off-body channel can be considered as a single-tap channel, and its pathloss model is free space model. The reasons are as follows: (1) the WiMax off-body channel in our cases is a line-of-sight channel; (2) the distance between WiMax TX and WiMax RX is far, the two antennas

are in the far field regions; (3) the influences of human body to UWB RX characteristics are all concluded and considered in the gain patterns of UWB RX antenna. However, as for UWB on-body channel, because of the wide bandwidth of UWB and the highly frequency-selective characteristic in the UWB frequency band, the UWB on-body channel model consists of a pathloss model and a power delay profile model. These two UWB channel models are both developed by measurements with antennas mentioned above and will be used in our following simulations. Sections 2.1.1 to 2.1.3 are the details of the two UWB channels.

2.1.1. Measurement Setup

To develop the UWB on-body channel model, measurements are essential, which play an important part in exploring WBAN channel behavior. There is a key point that a miniaturized UWB antenna with good performance is needed. A miniaturized UWB antenna with good performance developed in [8] is chosen as our reference antenna with some material parameters modified (FR4 substrate thickness 1.5 mm and relative permittivity 4.4). Two identical antennas used for TX and RX are fabricated. Figure 1 and Figure 2 show the structure and return loss of the antennas placed on the surface of the body, respectively.

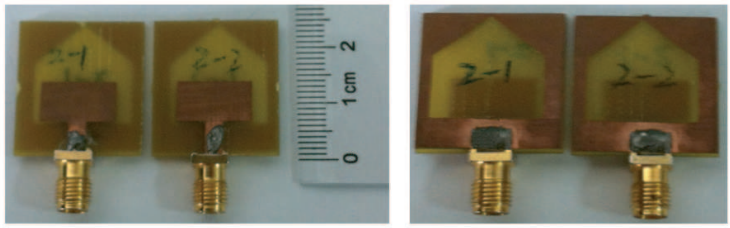

(a) (b)

Figure 1. Structure of the modified UWB antenna: (a) top view; (b) back view.

We measure the S_{21} parameter between the two antennas on a real adult human body by using a vector network analyzer (VNA). The measurements are performed in the frequency range from 3.1 GHz to 5.1 GHz in an indoor room. In the process of measurements, the body is in a standing position with arms hanging along the side. Specifications in this measurement on VNA and other equipments are listed in Table 1. The schematic diagram of the measurement is shown in Figure 3.

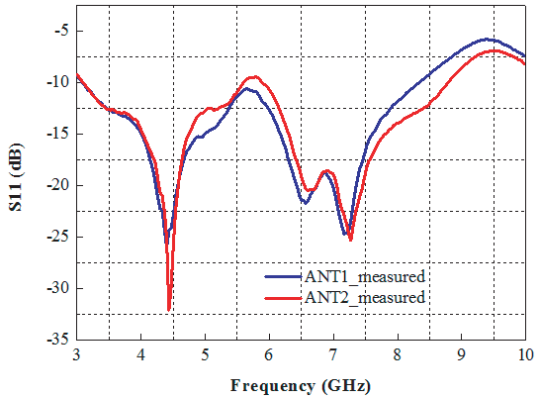

Figure 2. Return loss of the modified antenna.

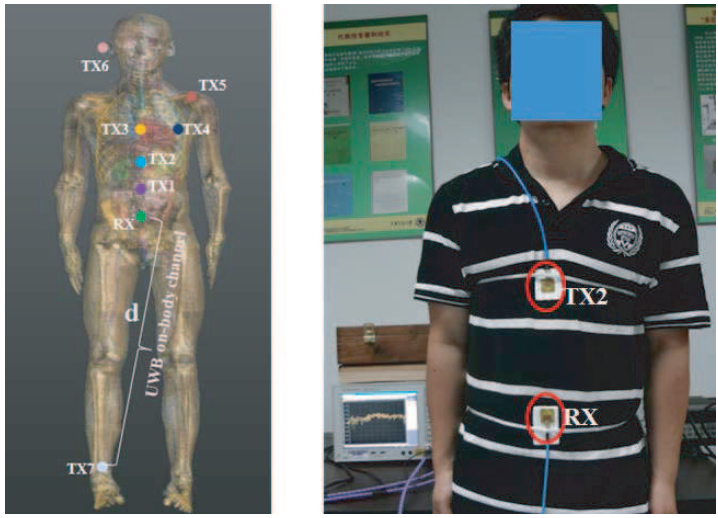

(a) (b)

Figure 3. Schematic diagram of the measurement: (a) TX and RX positions; (b) Indoor measurement.

2.1.2. UWB Pathloss Model

Due to the complexity of body and strong antenna-body interactions, EM wave propagation on-body will experience different processes, such as absorption, reflection, diffractions and etc, according to their TX and RX positions on-body. These make the UWB on-body channel to be quite different from the other traditional wireless one.

Table 1. Specifications in the measurement.

Equipment	Parameter	Value
VNA	VNA	Agilent E5071C
	Frequency range	3.1–5.1 GHz
	Number of points	1001
	Sweep time	Auto
	Calibration	Full-2-port (Tx power = 0 dBm)
	IF bandwidth	1 KHz
Human body	Gender	Male
	Height	175 cm
	Weight	70 kg
	Posture	Standing
Indoor room	Size	$8 \times 4 \times 4\,\mathrm{m}^3$
Antenna	Distance to body	5 mm
	Orientation	Head to head

In the processes of the measurements, the TX antenna is placed on the different parts of body surface, while the RX antenna is fixed on the navel of body, as shown in Figure 3. As summarized in Table 2, all the measurement positions are related to positions where sensors are attached to measure vital signs such as electrocardiogram (ECG), blood pressure, body temperature and so on. The distances between TX and RX are also listed in Table 2.

Table 2. The distance between TX and RX.

Position	Sensor	Distance d (TX-RX)/mm
TX1	ECG, Heart rate	100
TX2	ECG, Heart rate	200
TX3	ECG, Heart rate	300
TX4	ECG, Heart rate	320
TX5	Blood pressure	400
TX6	Body temperature	600
TX7	Acceleration	800

For each TX and RX position, we take 10 snapshots of S_{21}. The pathloss is obtained as mean path gain over the measured frequency band, as shown in the following equation

$$PL(d(p)) = -20 * \log_{10}\left\{\frac{1}{N_s}\frac{1}{N_f}\sum_{j=1}^{N_s}\sum_{n=1}^{N_f}\left|H_j^p(n)\right|\right\} \quad (1)$$

where $PL(d(p))$ is the pathloss at the position of p, at which the distance between TX and RX is denoted by $d(p)$. N_s and N_f are the number of the snapshots and frequency samples, respectively. $H_j^p(n)$ denotes the measured S_{21} for the position p, jth snapshot, and nth frequency sample. The path loss for each position is computed and plotted in Figure 4.

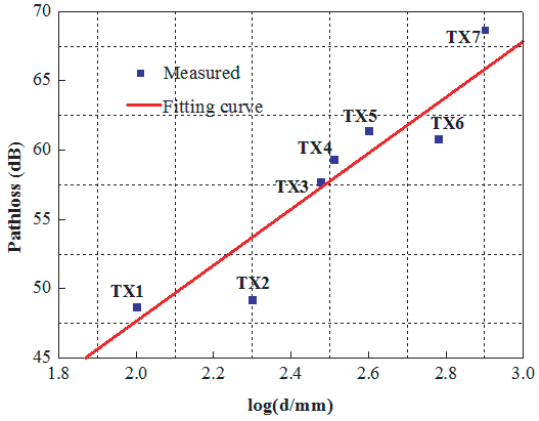

Figure 4. Pathloss of the measurements.

We model the pathloss model of on-body surface as a log-linear function of distance

$$PL(d) = a * \log(d) + b + N \quad (2)$$

where $PL(d)$ means the pathloss in dB at a distance d in mm, and a and b are the parameters derived by a least square fitting to the measured average pathloss. N is a stochastic term which has a log-normal distribution with zero-mean and standard deviation of σ_N. We get the pathloss parameters of our on-body channel model. The derived parameters are listed in Table 3.

2.1.3. UWB Power Delay Profile Model

Ten snapshots of position TX2 in frequency domain are shown in Figure 5. As we can see, position TX2 shows severe frequency selective

Table 3. Parameters of our measured on-body pathloss model.

Parameter	a	b	σ_N
Value	21.9	3.1	7.07

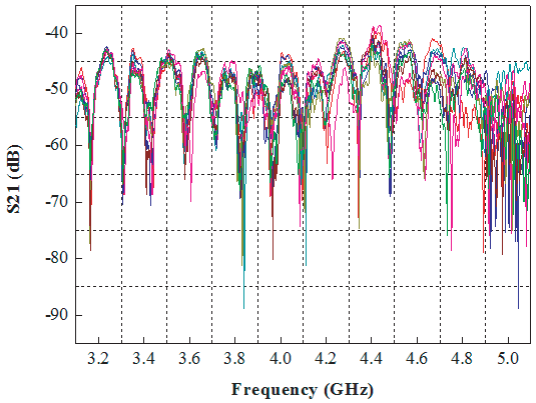

Figure 5. S_{21} in the frequency domain at position TX2.

fading. We convert the measured frequency domain data to time domain by a frequency hamming window and IFFT, then get the time domain channel impulse response (CIR). Peaks in each CIR are identified to use only the best paths for channel modeling. A threshold value that is 20 dB less than the amplitude of the strongest path is applied to the obtained local peaks. Then CIRs are normalized so that the amplitude of the first path is equal to one and the arrival time of the first path is 0 ns in each PDP. Figure 6 shows the path amplitude al derived from the measured data, together with the simple linear regression line.

The PDP model is given by a single cluster and exponential decay, and its power delay profile, $h(t)$, is modeled by

$$h_s(t) = \sum_{l=0}^{L-1} a_l \exp(j\varphi_l)\delta(t - t_l) \tag{3}$$

where a_l, t_l and φ_l denote the path amplitude, path arrival time, and phase for the l-th path, respectively. δ_l is the Dirac function, L stands for the number of the arrival paths. The phase φ_l is modeled by a uniform distribution over $[0,\ 2\pi)$. The path amplitude a_l is modeled

by an exponential decay Γ with a Rician factor γ_0, which is given by

$$10\log_{10}|a_l|^2 = \begin{cases} 0 & l = 0 \\ \gamma_0 + 10\log_{10}\left(\exp\left(-\frac{t_l}{\Gamma}\right)\right) + S & l \neq 0 \end{cases} \quad (4)$$

where S means a stochastic term modeled by a log-normal distribution with zero-mean and standard deviation of σ_S. The path arrival time t_l is modeled by Poisson distribution, which is written by

$$p(t_l\,|t_{l-1}) = \lambda\exp(-\lambda(t_l - t_{l-1})) \quad (5)$$

where λ means path arrival rate. The number of the arrival paths L is modeled by Poisson distribution, which is written by

$$p(L) = \frac{L_{av}^L\exp(L_{av})}{L!} \quad (6)$$

where L_{av} stands for the average of the L.

Parameters of our measured PDP model are summarized in Table 4.

Table 4. Parameters of PDP channel.

Parameters		Values
a_l	$\boldsymbol{\gamma_0}$	-8 dB
	$\boldsymbol{\Gamma}$	21.7
	$\boldsymbol{\sigma_s}$	7.39 dB
t_l	$\boldsymbol{\lambda}$	1.74 ns
L	L_{av}	16.5

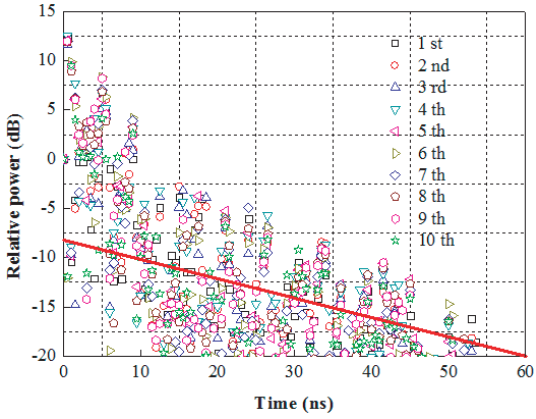

Figure 6. Exponential decay derived from the measured results.

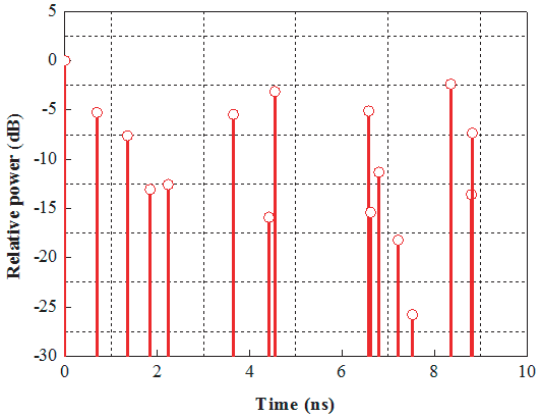

Figure 7. PDP model of UWB on-body channel.

According to the statistical parameters listed in Table 4, we obtain a concrete PDP model, as shown in Figure 7. This on-body PDP model, together with the pathloss model presented in Section 2.1.2, are the basis of our on-body UWB system performance evaluation.

2.2. Dual-mode Signal Model

In this section, we describe the dual-mode model of our UWB and WiMax system, as shown in Figure 8. In the system, a dual-mode signal model with the orthogonal frequency division multiplexing (OFDM) modulation is introduced. The multi-path UWB on-body channel has been measured in Section 2.1. Due to the fact that the WiMax off-body channel in our cases is a line-of-sight channel, the signal power only in a single-tap of this off-body channel is considered here.

2.2.1. UWB Signal Model

The UWB transmitted signal [29, 30] is given by

$$s_s(t) = \sum_{q=-\infty}^{\infty} \sum_{k=0}^{N_s-1} x_{k,q}\phi_k(t - qT_s)e^{j2\pi f_s t} \tag{7}$$

where N_s, T_s, and f_s are the number of subcarriers, OFDM symbol duration, and carrier frequency, respectively. As we know, the higher order modulation method adopted, the higher data rate but also the higher of error of the performance which could be defined by the transmitting distance on the body. In weighing up the data rate

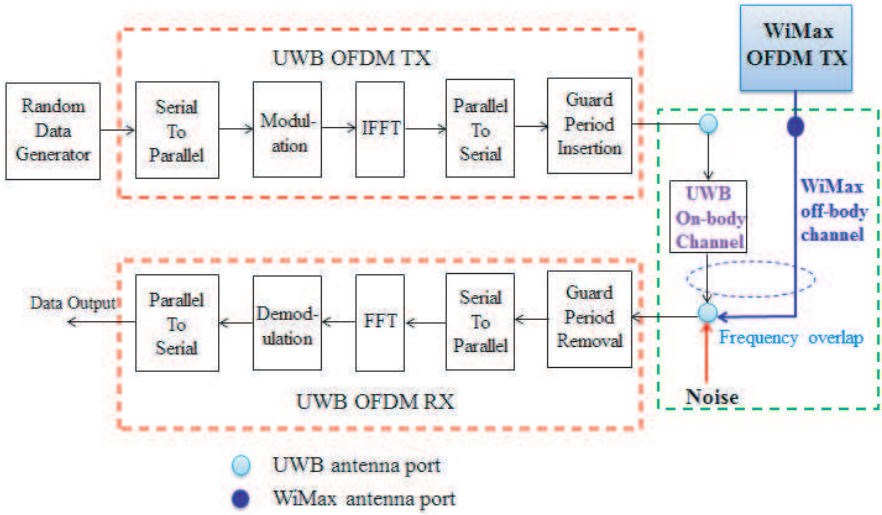

Figure 8. The dual-mode system.

and the transmitting distance on body, only the QPSK modulation is chosen. The transmitted QPSK symbols are denoted by $x_{k,q}$, where k and q represent the subcarrier index and the OFDM symbol index, respectively. The basic function of subcarrier k is given by

$$\phi_k(t) = \begin{cases} \frac{1}{\sqrt{D_s}} e^{j2\pi Q_s k(t-C_s)} & \text{if } t \in [0, T_s] \\ 0 & \text{else} \end{cases} \tag{8}$$

where C_s, $D_s = T_s - C_s$, W_s and $Q_s = W_s N_s$ are the duration of the guard interval, the data-carrying part of the OFDM symbol, the bandwidth of transmission, and the bandwidth per subcarrier, respectively.

2.2.2. WiMax Signal Model

The OFDM-WiMax transmitted signal is given by

$$s_i(t) = \sum_{l=-\infty}^{\infty} \sum_{m=0}^{N_i-1} z_{m,l} \theta_m(t - lT_i) e^{j2\pi f_i t} \tag{9}$$

where the modulated symbols are denoted by $z_{m,l}$. Only the QPSK modulation is chosen here. All parameters with subscript i are defined similarly as the equivalent UWB parameters with subscript s. The

basic function of subcarrier m is given by

$$\theta_m(t) = \begin{cases} \frac{1}{\sqrt{D_i}} e^{j2\pi Q_i k(t-C_i)} & \text{if } t \in [0, T_i] \\ 0 & \text{else} \end{cases} \tag{10}$$

2.2.3. Dual-mode System Model

It is well known that the UWB operates in 3.1–10.6 GHz while the WiMax in 3.4–3.6 GHz. Therefore, there are some spectrum overlaps of them, just as shown in Figure 5.

As shown in Figure 9, the WiMax transmitting signal $S_i(t)$, will come into on-body UWB RX through its spatial off-body channel $h_i(t)$. This signal will be able to affect the UWB system as interference, which leads to the performance degradations of the later. Due to the fact that the off-body channel in our cases is a line-of-sight channel, the signal power only in a single-tap of the off-body channel is considered here. In this case, the WiMax signal can be described as

$$S_{\text{Wimax}}(t) = S_i(t) \otimes \left[h_i(t) e^{-j\pi f_s t} \right] \tag{11}$$

where in (11), $h_i(t) = Ae^{j^{\alpha}\delta}(t-\tau)$ presents the single-tap channel with amplitude A and phase offset α, where α is uniformly distributed in [0, 2π], and τ denotes its time delay which is uniformly distributed on [0, T_i].

When the UWB transmitted signal $S_s(t)$ passes through its on-body channel defined by impulse response $h_s(t)$ and path loss $PL(d)$, the received UWB signals can be written by

$$S_{\text{UWB}}(t) = \{S_s(t) \otimes [-PL(d)h_s(t)]\} \tag{12}$$

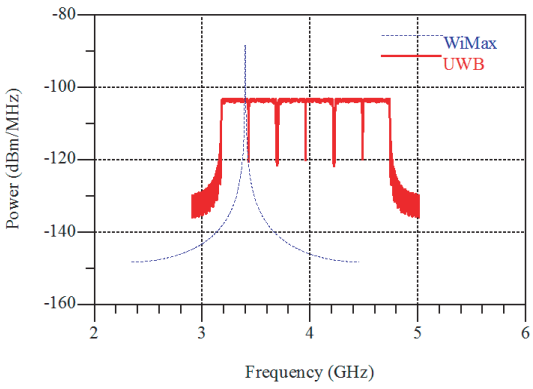

Figure 9. Spectrum overlap of WiMax and UWB.

where $PL(d)$ and $h_s(t)$ are the measured pathloss model and PDP model given in Section 2.1, respectively.

Because the bandwidth of the WiMax signal is very narrow compared with that of UWB signal, it is reasonable to consider that for the DL-DM communications the dual-mode received signals on-body at the UWB RX, consisted of the UWB signal and the WiMax one, can be modeling additively as

$$\begin{aligned} r(t) &= S_{\mathrm{UWB}}(t) + S_{\mathrm{Wimax}}(t) + n(t) \\ &= \left\{ \sum_{q=-\infty}^{\infty} \sum_{k=0}^{N_s-1} x_{k,q}\phi_k(t - qT_s)e^{j2\pi f_s t} \otimes [-PL(d)h_s(t)] \right\} \\ &\quad + \left\{ \sum_{l=-\infty}^{\infty} \sum_{m=0}^{N_i-1} z_{m,l}\theta_m(t - lT_i)e^{j2\pi f_i t} \otimes \left[h_i(t)e^{-j\pi f_s t} \right] \right\} + n(t) \end{aligned} \quad (13)$$

where in (13), $n(t)$ is the complex additive white Gaussian noise (AWGN). $S_{\mathrm{UWB}}(t)$ is the UWB signal at the UWB receiver which passed through the human body, and $S_{\mathrm{Wimax}}(t)$ is the WiMax signal at the UWB receiver which passed through the WiMax channel which is composed of free pathloss and different kinds of penetration loss. The final performance of the UWB on-body system is determined by the relative power level of $S_{\mathrm{UWB}}(t)$ to $S_{\mathrm{Wimax}}(t)$.

3. PERFORMANCE AND ANALYSIS

In Section 3, based on the two UWB on-body channel model derived and the dual-model signal model described above, we evaluate the performance of UWB on-body communication system and the performance under the WiMax off-body EMI. In the processes of simulation, to get a comprehensive understanding of the performance, different UWB data rates and several WiMax interference power levels at UWB receiver are considered.

3.1. Simulation Schematic Diagram and Conditions

The schematic diagram of simulation is shown in Figure 10, where $h_s(t)$ is the on-body channel measured in Section 2.1. $h_i(t)$ is WiMax channel. $S_s(t)$, $S_i(t)$, and $r(t)$ are just the signals described in Section 2.2.

The conditions of UWB and WiMax systems adopted in our simulation are listed in Table 5.

Some parameters of UWB and WiMax system layer are added in Table 6.

3.2. Performance Evaluation

To evaluate the performance of UWB on-body communication system under the WiMax interference, three vital factors are required carefully considered. The three factors are: (1) The UWB data transmitting rate r. (2) The UWB data transmitting distance d. (3) The WiMax interference power I at UWB receiver. r is inversely proportional to d, bigger r corresponds to smaller d. What I UWB received has a great impact on its performance reflected on the BER (no more than 10^{-3}) of the UWB system.

The WiMax off-body channel in our simulation is free space pathloss channel, and its pathloss can be described as

$$\begin{aligned} PL_{\text{WiMax}}(d_{\text{WiMax}}) &= -27.6 + 20 * \log(f_{\text{WiMax}}/\text{MHz}) \\ &\quad +20 * \log(d_{\text{WiMax}}/\text{m}) \\ &= 43.03 + 20 * \log(d_{\text{WiMax}}/\text{m}) \end{aligned} \tag{14}$$

Considering the typical EIRP (about 33 dBm) and wall

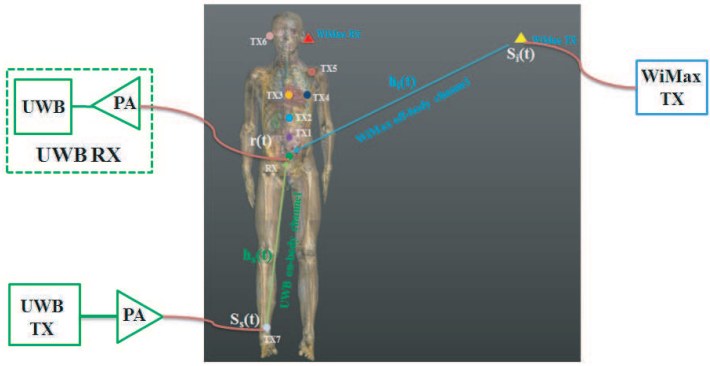

Figure 10. Simulation schematic.

Table 5. Conditions of UWB and WiMax OFDM systems.

UWB		WiMax	
N_s	128	N_i	256
W_s	528 MHz	W_i	10 MHz
T_s	312.5 ns	T_i	32 µs
C_s	70.07 ns	C_i	6.4 µs
D_s	242.43 ns	D_i	25.6 µs
Q_s	4.125 MHz	Q_i	0.039 MHz

penetration loss (about 16 dB), we compute some d_{WiMax} (m) for I (dBm) under different WiMax propagation environments. The computed results are shown in Table 7. Among the table, d_{WiMax} is the distance between WiMax terminal and UWB receiver, n is the number of the walls between them.

The simulated results of 480 Mbps UWB under WiMax EMI are shown in Figure 11, which indicates the relationship between the BER and d (distance between UWB TX and RX antenna) under different I when the UWB data transmitting rate r equals 480 Mbps. Without loss of generality, we set the threshold value of BER is 10^{-3} (when the

Table 6. Parameters of UWB and WiMax system layer.

UWB	
Frequency	3168–4752 MHz
Transmitting power	−9.9 dBm
Channel models	On-body channel model
Data length	1024

WiMax	
Carrier frequency	3.4 GHz
Channel model	AWGN
Path loss model	Free space model
Power at the UWB receiver receiver	−80 to −40 dBm

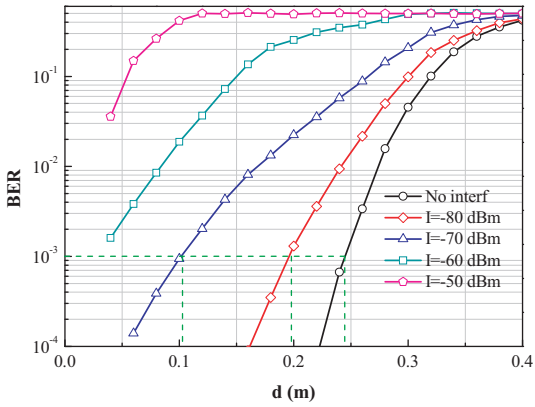

Figure 11. Simulated results of 480 Mbps UWB under WiMax EMI.

Table 7. Relationships between d_{WiMax}, n, and I.

d_{WiMax} \ I / n	−80	−70	−60	−50	−40
0	3151.4	996.6	315.1	99.7	31.5
1	499.5	157.9	49.9	15.8	5.0
2	79.1	25.03	7.9	2.5	0.8
3	12.5	4.0	1.3	0.4	0.1

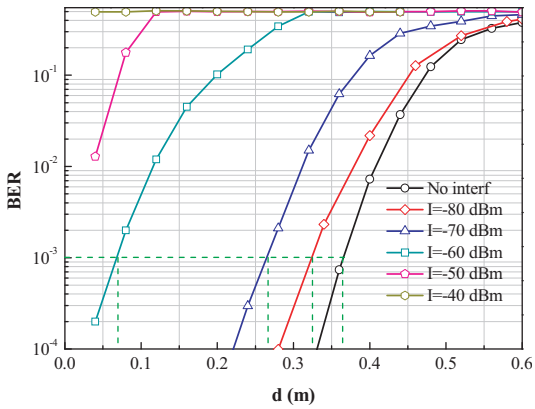

Figure 12. Simulated results of 320 Mbps UWB under WiMax EMI.

UWB transmitting data can be correctly received). For r is 480 Mbps, from Figure 11, we know that:

(1) When there is no WiMax interference, d is 0.245 m.

(2) When I equals −80, −70 dBm, d reduces to 0.2, 0.105 m respectively. And when I equals −60, −50 dBm, d almost equals 0! That is to say, when I equals −80, −70, −60, −50 dBm, Δd (the loss of d) is 0.045, 0.14, 0.245, 0.245 m, respectively.

For r is 320, 160, 80 Mbps, the simulated results are shown in Figures 12 to 14.

Due to the similarity of the 480 Mbps, the details of the analysis for 320, 160, and 80 Mbps are not presented here. All the analyzed results are arranged in Table 8.

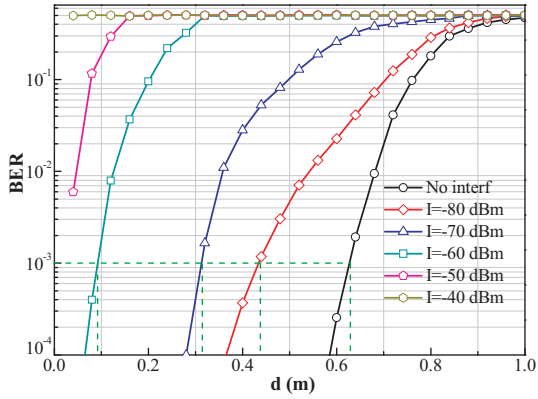

Figure 13. Simulated results of 160 Mbps UWB under WiMax EMI.

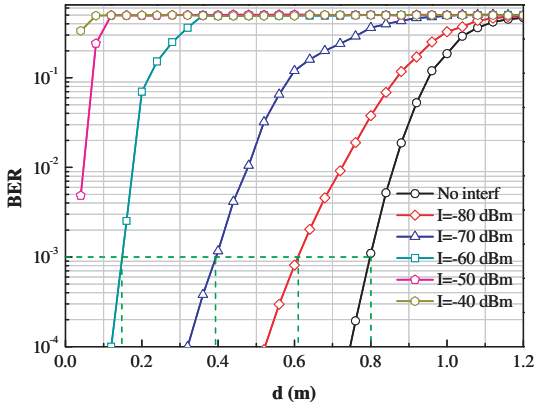

Figure 14. Simulated results of 80 Mbps UWB under WiMax EMI.

Table 8. Results for 480, 320, 160, 80 Mbps UWB under WiMax EMI.

Interf \ r		480 Mbps		320 Mbps		160 Mbps		80 Mbps	
		d (m)	Δd (m)	d (m)	Δd (m)	d (m)	Δd (m)	d (m)	Δd (m)
No interf		0.245	0	0.363	0	0.625	0	0.80	0
I	−80 dBm	0.20	0.045	0.33	0. 033	0.44	0.185	0.61	0.19
	−70 dBm	0.105	0.14	0.27	0.093	0.31	0.315	0.40	0.4
	−60 dBm	0	0.245	0.07	0.293	0. 09	0.535	0.15	0.65
	−50 dBm	0	0.245	0	0.363	0	0.625	0	0
	−40 dBm	0	0.245	0	0.363	0	0.625	0	0

3.3. Results Analysis

From Table 8, we know that when there is no WiMax EMI, transmission distance d equals 0.245, 0.363, 0.625, and 0.80 m for 480, 320, 160, and 80 Mbps data rate, respectively. The smaller r is, the further transmission distance d can we obtain. As shown in Figure 3 and Table 2, if we choose the upper part of the body as the TX and RX area, only 160 and 80 Mbps UWB on-body system can cover the transmission distance. When whole body is used for TX and RX area, only 80 Mbps system can achieve the communication.

When the WiMax off-body EMI exists, there is a sharp decline of the UWB transmission distance d. Take $n = 0$ and $n = 1$ two cases for example. For the former, 480, 320, 160, and 80 Mbps UWB can cover 0.20, 0.33, 0.44, and 0.61 m transmission distance, as long as the d_{WiMax} (distance between WiMax terminal and UWB receiver) is bigger than 3151.4 m. However, if the d_{WiMax} is 996.6 m, 480, 320, 160, and 80 Mbps UWB can only cover 0.105, 0.27, 0.31, and 0.40 m transmission distance. As the d_{WiMax} descends, the d falls sharply. For the latter $n = 1$, because of the loss of the wall, d can get some degree of improvement. 480, 320, 160, and 80 Mbps UWB cover 0.105, 0.27, 0.31, and 0.40 m, so long as d_{WiMax} does not exceed 499.5 m. As the n increases, the improvement of d is appreciable and it denotes the elevation of the anti-interference ability of UWB on-body system. Some other similar analysis can also be concluded just like above.

4. CONCLUSION

In this paper, a UWB on-body communication system and its WiMax EMI scenario are established and researched. A miniaturized UWB antenna is adopted to measure the on-body channel model. On the basis of the measured on-body channel model, we investigate the transmission performance and anti-interference ability of the on-body UWB system. Simulated results show that the transmission distance of on-body UWB system is quite limited and can be greatly influenced by WiMax EMI. However, this interference can be mitigated by some means, such as moving the WiMax equipments away from the UWB system, optimizing the capability of UWB receiving filter and improving the isolation between the UWB RX and WiMax TX antennas. The conclusions and suggestions in this paper have major significance in the applications of UWB spectrum planning, WBAN-UWB communication and UWB/WiMax double-mode coexistence.

ACKNOWLEDGMENT

This work was supported by the Major National S&T Program of China under Grant of 2011ZX03001-003-02, 2011ZX03003-001-03 and 2012ZX 03003-002-003.

REFERENCES

1. http://www.ieee802.org/15/pub/TG6.html.
2. Astrin, A. W., H.-B. Li, and R. Kohno, "Standardization for body area networks," *IEICE Trans. Commun.*, Vol. E92-B, No. 2, 366–372, Feb. 2009.
3. Kohno, R., K. Hamaguchi, H.-B. Li, and K. Takizawa, "R&D and standardization of body area network (BAN) for medical healthcare," *Proc. IEEE Int. Conf. on Ultra-Wideband, (ICUWB)*, Vol. 3, 5–8, Sep. 2008.
4. Chen, D. and C.-H. Cheng, "A novel compact ultra-wideband (UWB) wide slot antenna with via holes," *Progress In Electromagnetics Research*, Vol. 94, 343–349, 2009.
5. Haga, N., K. Saito, M. Takahashi, and K. Ito, "Characteristics of cavity slot antenna for body-area networks," *IEEE Trans. Antennas Propag.*, Vol. 57, No. 4, 837–843, Apr. 2009.
6. Gemio, J., J. Parron, and J. Soler, "Human body effects on implantable antennas for ISM bands applications: Models comparison and propagation losses study," *Progress In Electromagnetics Research*, Vol. 110, 437–452, 2010.
7. Zhang, M. and A. Alden, "Calculation of whole-body SAR from a 100 MHz dipole antenna," *Progress In Electromagnetics Research*, Vol. 119, 133–153, 2011.
8. Vidal, N., S. Curto, J. M. Lopez-Villegas, J. Sieiro, and F. M. Ramos, "Detuning study of implantable antennas inside the human body," *Progress In Electromagnetics Research*, Vol. 124, 265–283, 2011.
9. Jin, X. and M. Ali, "Embedded antennas in dry and saturated concrete for application in wireless sensors," *Progress In Electromagnetics Research*, Vol. 102, 197–211, 2010.
10. Smith, D. B., D. Miniutti, and L. W. Hanlen, "Characterization of the body-area propagation channel for monitoring a subject sleeping," *IEEE Trans. Antennas Propag.*, Vol. 59, No. 11, 4388–4392, Nov. 2011.
11. Astrin, A. W., H.-B. Li, and R. Kohno, "Standardization for body

area networks," *IEICE Trans. Commun.*, Vol. E92-B, No. 2, 366–372, Feb. 2009.

12. Abbasi, Q. H., A. Sani, A. Alomainy, and Y. Hao, "Arm movements effect on ultra wideband on-body propagation channels and radio systems," *Antennas Propag. Conf.*, 261–264, Loughborough, U.K., Nov. 2009.
13. Abbasi, Q., A. Alomainy, and Y. Hao, "Effect of human body movements on performance of multiband OFDM based ultra wideband wireless communication system," *Antennas Propag. Conf.*, 145–148, Loughborough, UK, Nov. 2010.
14. Porcino, D. and W. Hirt, "Ultra-wideband radio technology: Potential and challenges ahead," *IEEE Commun. Mag.*, Vol. 41, No. 7, 66–74, Jul. 2003.
15. Cardinali, R., L. D. Nardis, D. Benedetto, and M.-G. Lombardo, "UWB ranging accuracy in high- and low-data-rate applications," *IEEE Trans. Microw. Theory Tech.*, Vol. 54, No. 4, 1865–1875, Jun. 2006.
16. Azim, R., M. T. Islam, and N. Misran, "Compact tapered-shape slot antenna for UWB applications," *IEEE Antennas Wireless Propag. Lett.*, Vol. 10, 1190–1193, 2011.
17. Chahat, N., M. Zhadobov, and R. Sauleau, "A compact UWB antenna for on-body applications" *IEEE Trans. Antennas Propag.*, Vol. 59, No. 4, 1123–1131, Apr. 2011.
18. Habib, M. A., A. Bostani, A. Djaiz, M. Nedil, M. C. E. Yagoub, and T. A. Denidni, "Ultra wideband CPW-FED aperture antenna with WLAN band rejection," *Progress In Electromagnetics Research*, Vol. 106, 17–31, 2010.
19. Xu, H.-Y., H. Zhang, K. Lu, and X.-F. Zeng, "A holly-leaf-shaped monopole antenna with low RCS for UWB application," *Progress In Electromagnetics Research*, Vol. 117, 35–50, 2011.
20. Li, C.-M. and L.-H. Ye, "Improved dual band-notched UWB slot antenna with controllable notched bandwidths," *Progress In Electromagnetics Research*, Vol. 115, 477–493, 2011.
21. Islam, M. T., R. Azim, and A. T. Mobashsher, "Triple band-notched planar UWB antenna using parasitic strips," *Progress In Electromagnetics Research*, Vol. 129, 161–179, 2011.
22. Sim, C.-Y.-D., W.-T. Chung, and C.-H. Lee, "Planar UWB antenna with 5 GHz band rejection switching function at ground plane," *Progress In Electromagnetics Research*, Vol. 106, 321–333, 2010.
23. Hu, Y.-S., M. Li, G.-P. Gao, J.-S. Zhang, and M.-K. Yang,

"A double-printed trapezoidal patch dipole antenna for UWB applications with band-notched characteristic," *Progress In Electromagnetics Research*, Vol. 103, 259–269, 2010.

24. Wang, Q., T. Tayamachi, and I. Kimura, "An on-body channel model for UWB body area communications for various postures," *IEEE Trans. Antennas Propag.*, Vol. 57, No. 4, 991–998, Apr. 2009.
25. Zhao, Y., Y. Hao, A. Alomainy, and C. Parini, "UWB on-body radio channel modeling using ray theory and subband FDTD method," *IEEE Trans. Microw. Theory Tech.*, Vol. 54, No. 4, 1827–1835, Apr. 2006.
26. Sani, A., A. Alomainy, G. Palikaras, and Y. Nechayev, "Experimental characterization of UWB on-body radio channel in indoor environment considering different antennas," *IEEE Trans. Antennas Propag.*, Vol. 58, No. 1, 238–241, Jan. 2010.
27. Takizawa, K., T. Aoyagi, and R. Kohno, "Channel modeling and performance evaluation of UWB-based wireless body area networks," *Proc. IEEE ICC*, 1–5, 2009.
28. Hernandez, M. and R. Kohno, "Coexistence of UWB-BANs with other wireless systems," *Proc. IEEE Int. Conf. on Intelligent Signal Processing and Communication Systems, (ISPACS)*, 135–137, Jan. 2009.
29. You, Y. H. and J. B. Kim, "Pilot and data symbol-aided frequency ESTI-mation for UWB-OFDM," *Progress In Electromagnetics Research,* Vol. 90, 205–217, 2009.
30. Chen, Z. and Y.-P. Zhang, "Effects of antennas and propagation channels on synchronization performance of a pulse-based ultra-wideband radio system," *Progress In Electromagnetics Research*, Vol. 115, 95–112, 2011.